Supplementary information:

X-ray stability and degradation mechanism of lead halide perovskites and lead halides

Sebastian Svanström[1], Alberto Garcia Fernandez[2], Tamara Sloboda[2], T. Jesper Jacobsson[3], Håkan Rensmo[1], Ute B. Cappel[2*]

1: Division of X-ray Photon Science, Department of Physics and Astronomy, Uppsala University, Box 516, SE-751 20, Uppsala, Sweden

2: Division of Applied Physical Chemistry, Department of Chemistry, KTH - Royal Institute of Technology, SE-100 44 Stockholm, Sweden

3: Young Investigator Group Hybrid Materials Formation and Scaling, Helmholtz-Zentrum Berlin für Materialen und Energie GmbH, Albert-Einstein Straße 16, 12489 Berlin, Germany

* cappel@kth.se

Table of contents

X-ray flux densities

Table S1: The X-ray intensities, mirror current, flux densities, irradiance and pass energies used at I09 beamline at the DIAMOND light source.

Mirror current [nA]	Intensity [photons/s]	Flux density [photons/s/cm^2]	Irradiance [mW/cm^2]	Pass energy [eV]
1.48	$1.1x10^{11}$	$3.0x10^{13}$	1.42	200
2.9	$2.2x10^{11}$	$5.8x10^{13}$	2.79	200
5.9	$4.4x10^{11}$	$1.2x10^{14}$	5.67	200
11.9	$8.8x10^{11}$	$2.4x10^{14}$	11.4	100
23	$1.7x10^{12}$	$4.6x10^{14}$	22.1	100
47	$3.5x10^{12}$	$9.4x10^{14}$	45.2	50
98	$7.3x10^{12}$	$2.0x10^{15}$	94.2	50
135	$1.0x10^{13}$	$2.7x10^{15}$	130	-

Table S2: The X-ray flux density, irradiance and pass energies used at the Galaxies beamline at the SOLEIL synchrotron.

Beam current	450 mA			100 mA		
Filter transmission	Flux density [photons/s/cm^2]	Irradiance [mW/cm^2]	Pass energy [eV]	Flux density [photons/s/cm^2]	Irradiance [mW/cm^2]	Pass energy [eV]
0.21 %	$1.33x10^{14}$	6.34	200	$2.95x10^{13}$	1.42	500
0.42 %	-	-	-	$5.82x10^{13}$	2.80	500
1.44 %	-	-	-	$2.01x10^{14}$	9.68	500
1.81 %	$1.14x10^{15}$	54.8	200	-	-	-
5.10 %	$3.21x10^{15}$	154	100	-	-	-
11.47 %	$7.22x10^{15}$	347	100	$1.60x10^{15}$	77.1	100
22.58 %	$1.42x10^{16}$	683	50	-	-	-
50.69 %	$3.19x10^{16}$	1534	50	-	-	-
100.0 %	$6.30x10^{16}$	3026	50	$1.40x10^{16}$	672	-

Model for heating induced by an elliptical photon beam

The incoming power of a monochromatic photon (X-ray, UV or laser) beam can be calculated by

$$P_{\mathrm{ph}} = N_{\mathrm{ph}} E_{\mathrm{ph}} e$$

N_{ph} is the number of photons per second, e is the charge of the electron (1.60x10^{-19} C) and E_{ph} is the photon energy (in eV). This power input needs to be balanced by heat losses from the spot. The heat losses can be divided into two types, radiative and conductive.

The radiative losses can be calculated by assuming that both the spot and the surrounding are black bodies which allows the radiative balance to be calculated using

$$P_{\mathrm{rad}} = \sigma A_{\mathrm{spot}} (T_{\mathrm{spot}}^4 - T_{\mathrm{amb}}^4)$$

where σ is Stefan-Boltzmann constant (5.67x10^{-8} W m^{-2} K^{-4}), T_{spot} is the temperature of the spot, T_{amb} is the ambient temperature (20°C), and A_{spot} is the area of the spot which for an ellipse is ($A_{\mathrm{spot}} = \pi\, a\, b$) where a is the width of the spot and b is the length of the spot. The conduction losses in the substrate of an elliptical spot can be estimate by (half of) the heat conduction from an ellipsoid in an infinite medium, shown in Figure S1.

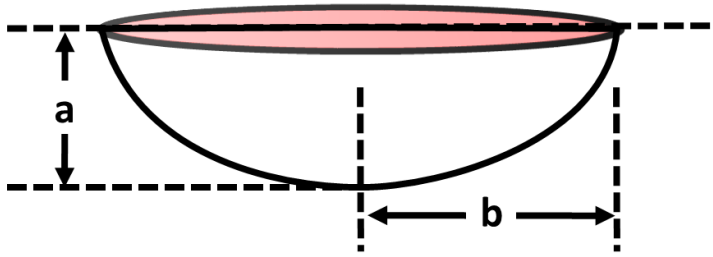

Figure S1: The heated shape modelled by an elliptical spot on the sample.

The heat losses from this shape can be calculated using

$$P_{\mathrm{cond}} = \frac{2\pi k (T_{\mathrm{spot}} - T_{\mathrm{amb}}) \sqrt{1 - a^2/b^2}}{\operatorname{arctanh} \sqrt{1 - a^2/b^2}}$$

where k is the heat conductivity (W/mK) of the substrate[1], in this case glass (0.8 W/m^2). This model requires that the width of the spot (a) is significantly larger than thickness of the thin film but significantly smaller than the thickness of the substrate. However, if the conductivity of the substrate is lower than of the surface to which it is mounted this calculation will still give a higher limit of the temperature. To calculate the temperature of the spot the energy balance can be calculated using

$$P_{\mathrm{ph}} = P_{\mathrm{rad}} + P_{\mathrm{cond}}$$

and solved for T_{spot}. The spot dimensions, maximum X-ray power and the resulting spot temperature (the ambient temperature is 20 °C) in the three measurement is shown in Table S3.

Table S3: The dimensions of the X-ray spot, maximum power and X-ray spot temperature.

	Diamond LS	SOLEIL (450 mA)	SOLEIL (100 mA)
Spot length (µm)	1570	3300	3300
Spot width (µm)	300	30	30
Max power (mW)	0.34	1.63	0.042
Spot temperature (°C)	20.4	22.8	20.1

Core to core binding energy differences

Table S4: The core to core binding energy differences in eV of the compounds used in this study.

	PbI_2	$PbBr_2$	$Cs_{0.17}FA_{0.73}PbI_3$	$Cs_{0.17}FA_{0.73}PbBr_{0.51}I_{2.49}$	$MA_{0.17}FA_{0.73}PbBr_{0.51}I_{2.49}$	$CsPbBr_3$
$Pb5d_{5/2}$ - $I4d_{5/2}$	-29.76		-29.73	-29.72	-29.71	
$Pb5d_{5/2}$ - $I3d_{5/2}$	-599.74		-599.68	-599.67	-599.67	
$Pb5d_{5/2}$ - $Br3d_{5/2}$		-48.59		-48.83	-48.92	-48.76
$Pb5d_{5/2}$ - $Cs4d_{5/2}$			-55.36	-56.24		-55.83
$Pb5d_{5/2}$ - $Cs3d_{5/2}$			-705.41	-705.29		-704.91
$Pb5d_{5/2}$ - N1s (FA^+)			-281.19	-381.07	-381.04	
$Pb5d_{5/2}$ - C1s (FA^+)			-268.88	-268.79	-268.73	
$Pb4f_{7/2}$ - $I4d_{5/2}$	89.03		89.12	89.14	89.15	
$Pb4f_{7/2}$ - $I3d_{5/2}$	-481.04		-480.85	-480.81	-408.79	
$Pb4f_{7/2}$ - $Br3d_{5/2}$		70.31		69.92	69.93	70.09
$Pb4f_{7/2}$ - $Cs4d_{5/2}$			62.49	62.63		63.02
$Pb4f_{7/2}$ - $Cs3d_{5/2}$			-586.57	-586.42		-586.09
$Pb4f_{7/2}$ - N1s (FA^+)			-262.34	-262.24	-262.20	
$Pb4f_{7/2}$ - C1s (FA^+)			-150.03	-149.93	-149.87	

Lead halides

Figures S2a and S2c show the Pb4f$_{7/2}$, Br3d, I4d core levels and valence band of the lead halides normalised and calibrated against Pb4f$_{7/2}$ (Pb^{2+} component). The Pb4f, Br3d and I4d core levels were fitted as described in the methods section in order to determine evolution of the percentage of Pb^{0} and the halide/Pb^{2+} ratio shown in Figures S2b and S2d.

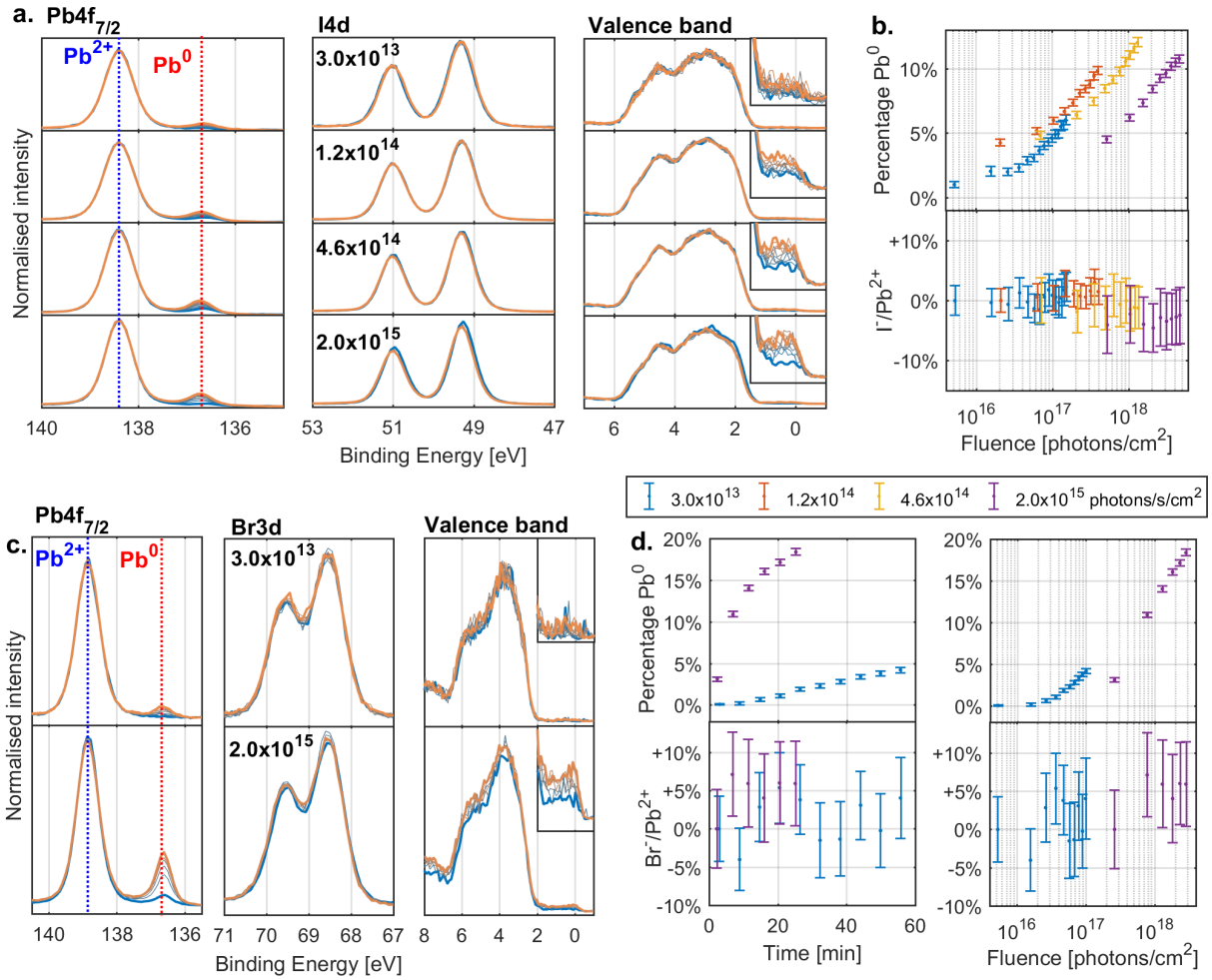

*Figure S2: **a**) The Pb4f$_{7/2}$, I4d and valence band (Fermi edge enlarged) spectra recorded for a PbI$_2$ sample as a function of time (blue: start, orange: end) and at different X-ray flux densities (units: photons/s/cm^2). **b**) Fraction of Pb^0 and relative change in iodide to Pb^{2+} ratio as a function of fluence for the PbI$_2$ sample. **c**) The Pb4f$_{7/2}$, Br3d and valence band (Fermi edge enlarged) spectra recorded for a PbBr$_2$ sample as a function of time (blue: start, orange: end) and at different X-ray flux densities (units: photons/s/cm^2). **d**) Fraction of Pb^0 and relative change in bromide to Pb^{2+} ratio as a function of time and fluence for the PbBr$_2$ sample. Measured at the I09 beamline at DIAMOND light source with a photon energy of 3000 eV and spectra in (a) and (c) were intensity normalised and energy calibrated against the Pb^{2+} component of the Pb4f.*

Organic lead halide perovskites

Spectrum and chemical ratios

Figures S3, S4a and S5 show the Cs3d$_{5/2}$, I3d$_{5/2}$, N1s, Pb4f$_{7/2}$, Br3d core levels and valence band of the MAFA-Mix ($MA_{0.17}FA_{0.83}PbBr_{0.49}I_{2.52}$), CsFA-Mix ($Cs_{0.17}FA_{0.83}PbBr_{0.49}I_{2.52}$) and CsFA-I samples normalised and calibrated against Pb4f$_{7/2}$ (Pb^{2+} component). The core levels of the CsFA-Mix sample were fitted as described in the methods section in order to determine the evolution of the Pb^0/Pb^{2+}, the Br$^-$/Pb^{2+}, I$^-$/Pb^{2+}, Cs$^+$/Pb^{2+}, and N(FA)/Pb^{2+} ratio shown in Figure S4b.

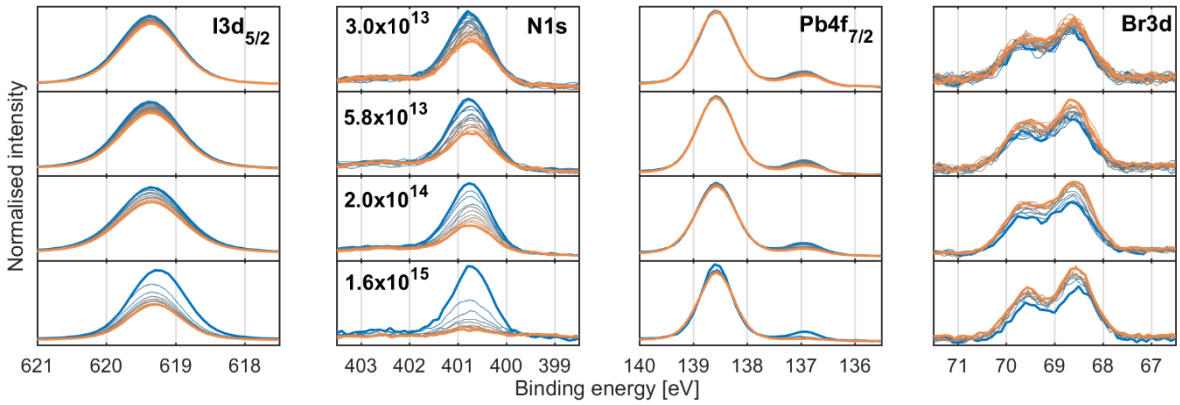

Figure S3: The $I3d_{5/2}$, N1s, $Pb4f_{7/2}$, Br3d spectra recorded for the MAFA-Mix ($MA_{0.17}FA_{0.83}PbBr_{0.49}I_{2.51}$) sample as a function of time (blue: start, orange: end) at different X-ray flux densities (units: photons/s/cm²). Intensity normalised and energy calibrated against the Pb^{2+} component of the Pb4f. Measured at SOLEIL, with a beam current of 100 mA, using a photon energy 3000 eV.

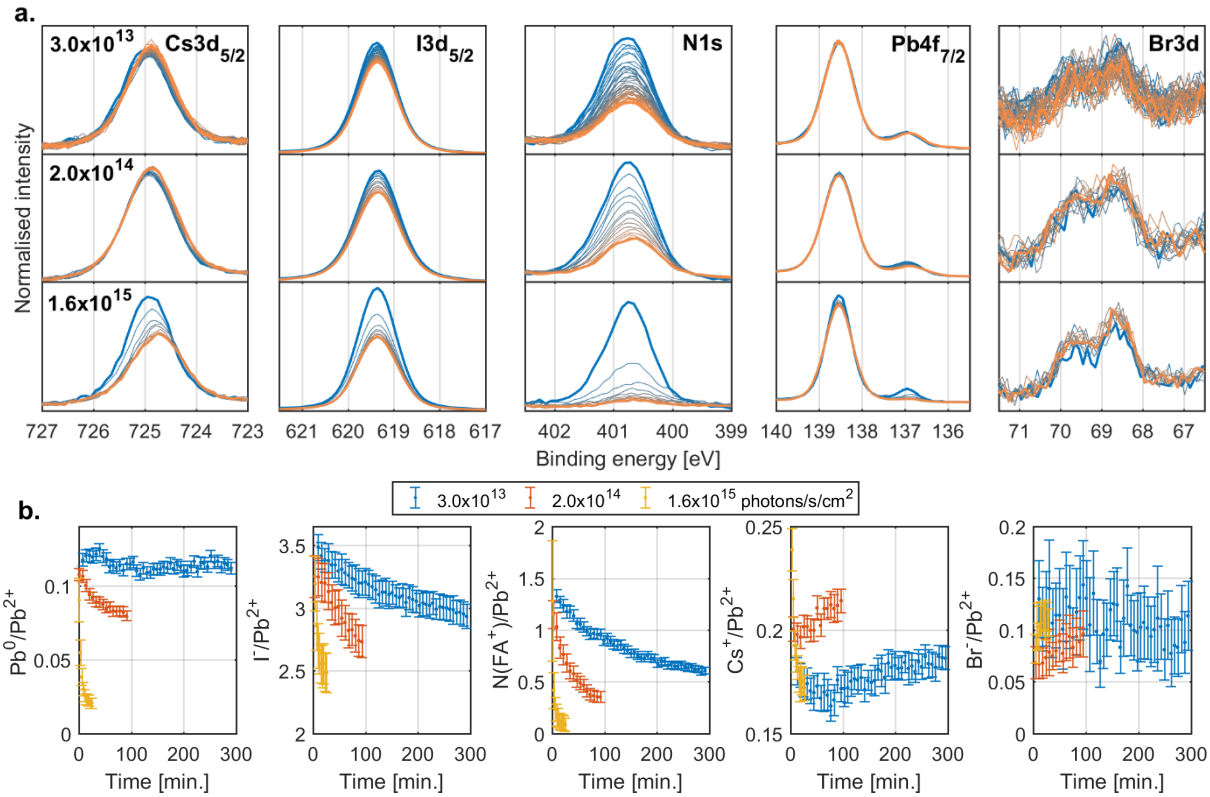

*Figure S4: **a**) The $Cs3d_{5/2}$, $I3d_{5/2}$, N1s, $Pb4f_{7/2}$, Br3d spectra recorded for a CsFA-Mix ($Cs_{0.17}FA_{0.83}PbBr_{0.49}I_{2.51}$) sample as a function of time (blue: start, orange: end) and at different X-ray flux densities (units: photons/s/cm²). Intensity normalised and energy calibrated against the Pb^{2+} component of Pb4f. Measured at SOLEIL, with a beam current of 100 mA, using a photon energy 3000 eV. **b**) The Pb^0/Pb^{2+}, I^-/Pb^{2+}, $N(FA)/Pb^{2+}$, Cs^+/Pb^{2+} and Br^-/Pb^{2+} ratios as a function time at different X-ray flux densities.*

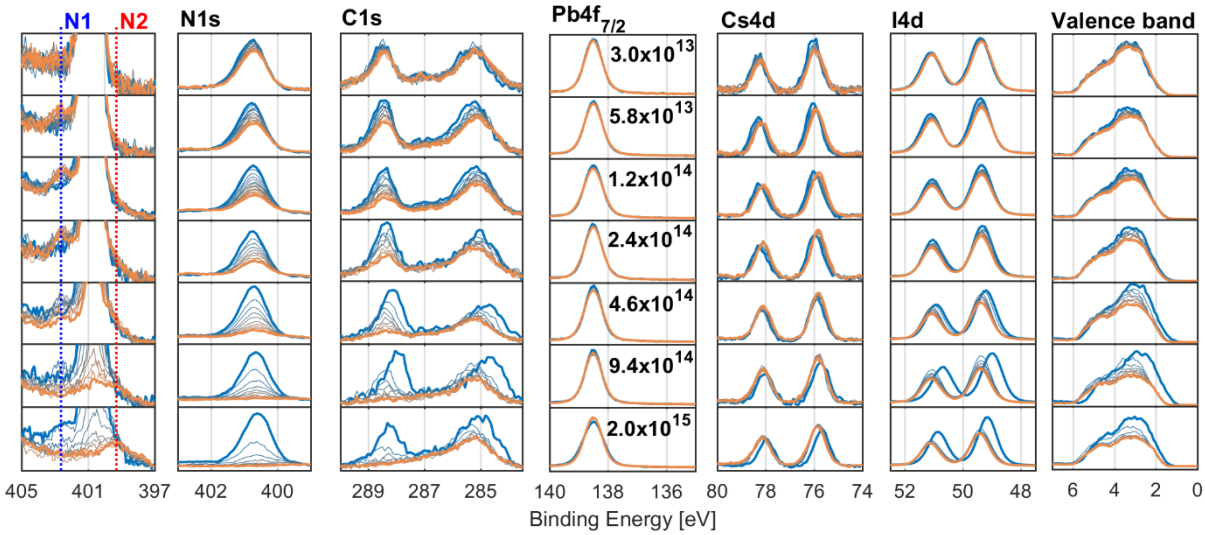

Figure S5: The N1s, C1s, Pb4f$_{7/2}$, Cs4d, I4d and valence band spectra recorded for a CsFA-I ($Cs_{0.17}FA_{0.83}PbI_3$) sample as a function of time (blue: start, orange: end) at different X-ray flux densities (units: photons/s/cm^2). Intensity normalised and energy calibrated against Pb^{2+} component of Pb4f. Measured at the I09 beamline at the DIAMOND light source using a photon energy 3000 eV.

Analysis of degradation kinetics

The I^-/Pb^{2+}, N(FA)/Pb^{2+} and C(FA)/Pb^{2+} ratios determined from measurements at all X-ray flux densities, of the CsFA-I, CsFA-Mix and MAFA-Mix samples were fitted with an exponential decay, shown in Equation 1. The resulting parameters, as well as the initial ratios R(0), are shown in Table S5 and the fits are shown in figure S6.

$$R(x) = R_0 e^{-k_r x} + R_\infty \qquad (1)$$

were R_0 is the change in ratio due to irradiation, R_∞ is the ratio after complete decay and k_r is the radiolysis constant of the decay. In the case of N(FA^+)/Pb^{2+}, C(FA^+)/Pb^{2+} the ratio after complete decay is fixed to 0.

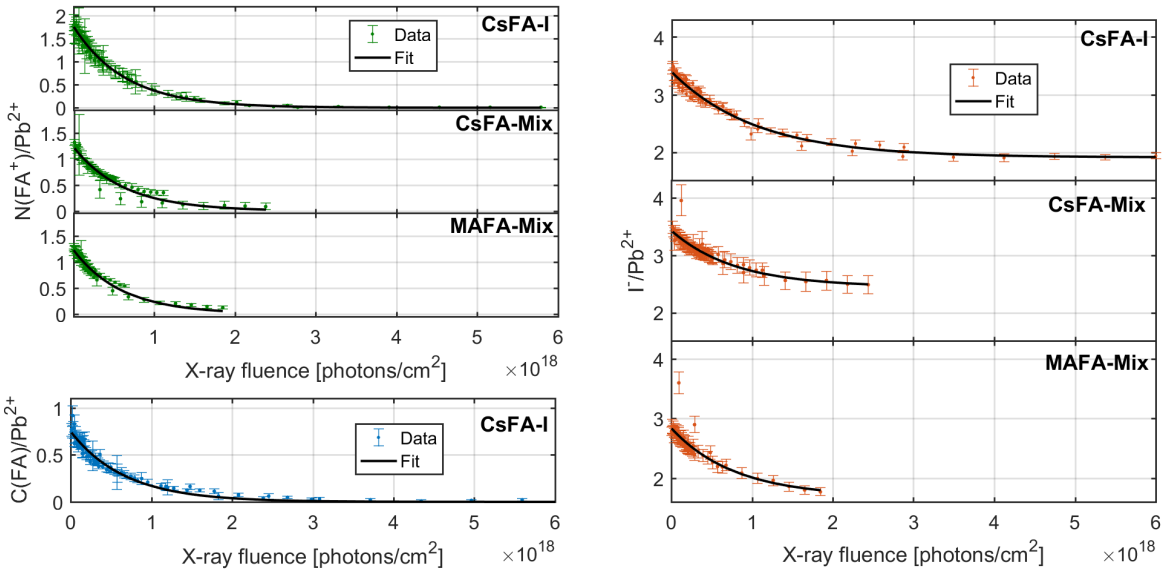

Figure S6: The exponential decay fit of I^-/Pb^{2+}, N(FA^+)/Pb^{2+} and C(FA^+)/Pb^{2+} ratio of the CsFA-I, CsFA-Mix and MAFA-Mix samples.

Table S5: The fitted exponential decay parameters for I^-/Pb^{2+}, $N(FA^+)/Pb^{2+}$ and $C(FA^+)/Pb^{2+}$ ratio for the CsFA-I, CsFA-Mix and MAFA-Mix.

Sample	Ratio	R_0	R_∞	k_r [cm^2/photon]	$R_0 + R_\infty$
CsFA-I	I^-/Pb^{2+}	1.48	1.91	$0.95x10^{-18}$	3.39
	$N(FA^+)/Pb^{2+}$	1.76	-	$1.56x10^{-18}$	1.76
	$C(FA^+)/Pb^{2+}$	0.75	-	$1.48x10^{-18}$	0.75
CsFA-Mix	I^-/Pb^{2+}	0.96	2.45	$1.28x10^{-18}$	3.41
	$N(FA^+)/Pb^{2+}$	1.21	-	$1.59x10^{-18}$	1.21
MAFA-Mix	I^-/Pb^{2+}	1.15	1.69	$1.28x10^{-18}$	2.84
	$N(FA^+)/Pb^{2+}$	1.24	-	$1.68x10^{-18}$	1.24

Chemical ratios vs. fluence

Figure S7-8 show the Pb^0/Pb^{2+}, I^-/Pb^{2+}, $N(FA^+)/Pb^{2+}$, Br^-/Pb^{2+} and Cs^+/Pb^{2+} ratios (where applicable) of the CsFA-I, CsFA-Mix and MAFA-Mix samples as a function of fluence. The exponential decay fit has been included as a guide for the eye.

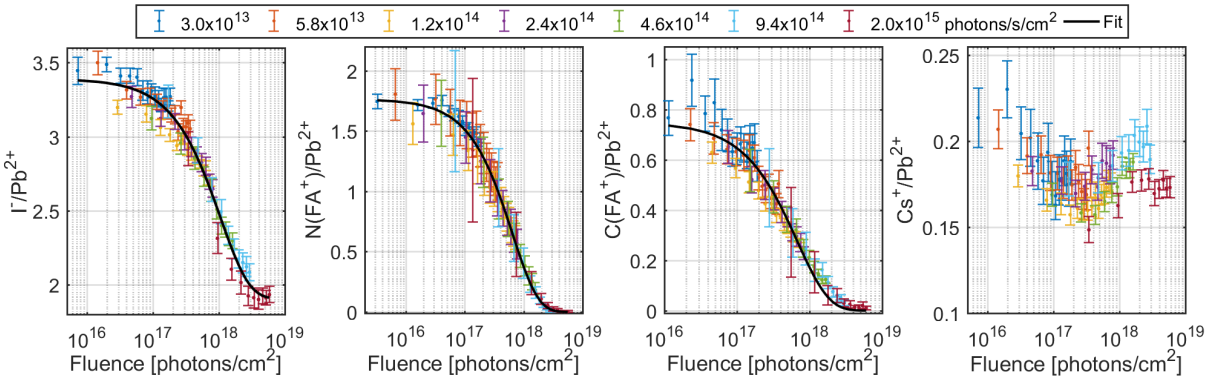

Figure S7: The I^-/Pb^{2+} (left), $N(FA)/Pb^{2+}$ (middle left), $C(FA)/Pb^{2+}$ (middle right) and Cs^+/Pb^{2+} (right) ratio of the CsFA-I sample as a function of X-ray fluence at different X-ray flux densities.

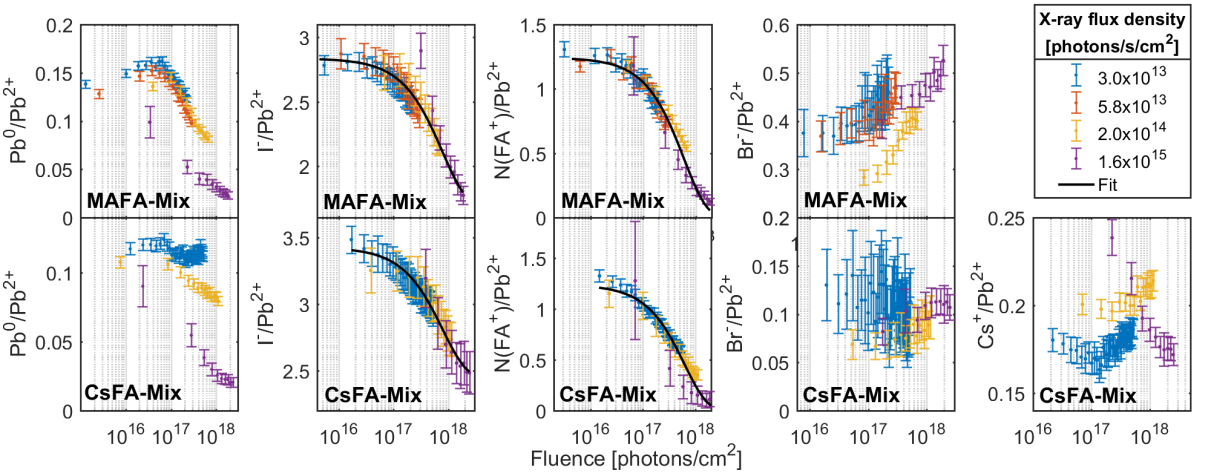

Figure S8: The Pb^0/Pb^{2+}, I^-/Pb^{2+}, $N(FA^+)/Pb^{2+}$, Br^-/Pb^{2+} and Cs^+/Pb^{2+} ratio of the MAFA-Mix and CsFA-Mix samples as a function of X-ray fluence at different X-ray flux densities.

$CsPbBr_3$

Spectrum and example fits

Figure S9 shows the Cs3d and Pb4f core levels while Figure S10 shows the C1s, Cs4d, Br3d, Pb5d core levels and valence band (Fermi level enlarged) of the $CsPbBr_3$ sample normalised and calibrated against total Pb4f signal intensity. Figure S11 show an example of the curve fits of Pb4f, Cs4d and Br3d after degradation has begun. Figure S12 shows the ratio of the initial components (Cs^+, Br^- and

$Pb2^{+}$) and the new components (Cs_{New}, Br_{New} and Pb^{0}) as a function of time and fluence. Figure S13a shows the ratio between the new Br3d and Cs4d components of the $CsPbBr_3$ sample. Figure S13b shows the Cs^{+}/Pb^{2+} and Br^{-}/Pb^{2+} ratio in the $CsPbBr_3$ sample as a function of time and fluence. Table S6 show the binding energies and core to core binding energy differences of the CsBr reference sample. Figure S14 show the fits of the Cs3d, Cs4d and Br3d core levels of the CsBr reference sample.

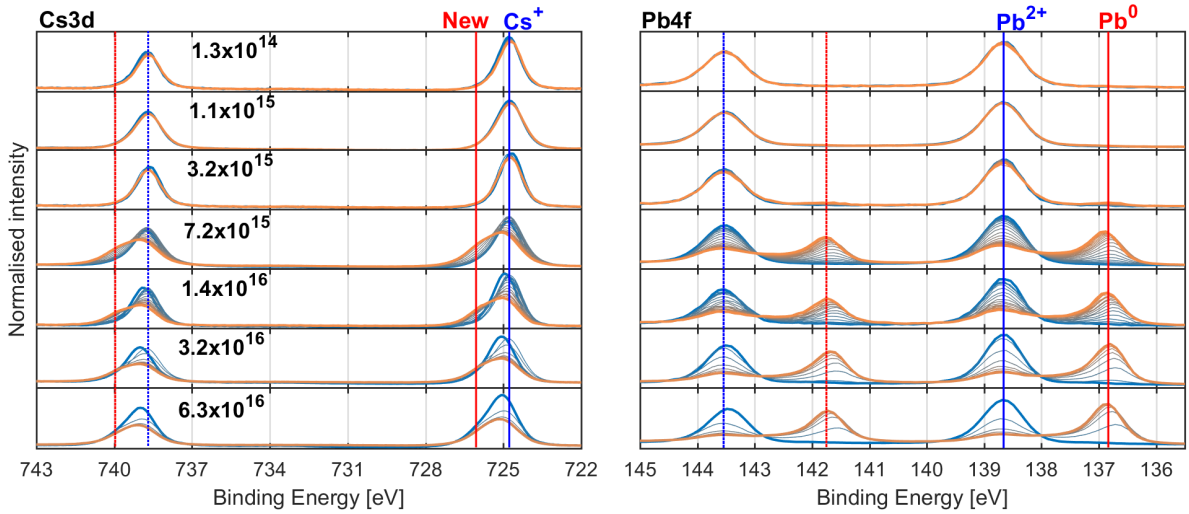

Figure S9: The Cs3d and Pb4f spectra recorded for a $CsPbBr_3$ sample as a function of time (blue: start, orange: end) and at different X-ray flux densities (units: photons/s/cm²) for the Cs3d and Pb4f normalised to total Pb4f and calibrated to total Pb4f at 138.7 eV. Measured at SOLEIL (450 mA) using a photon energy 3000 eV.

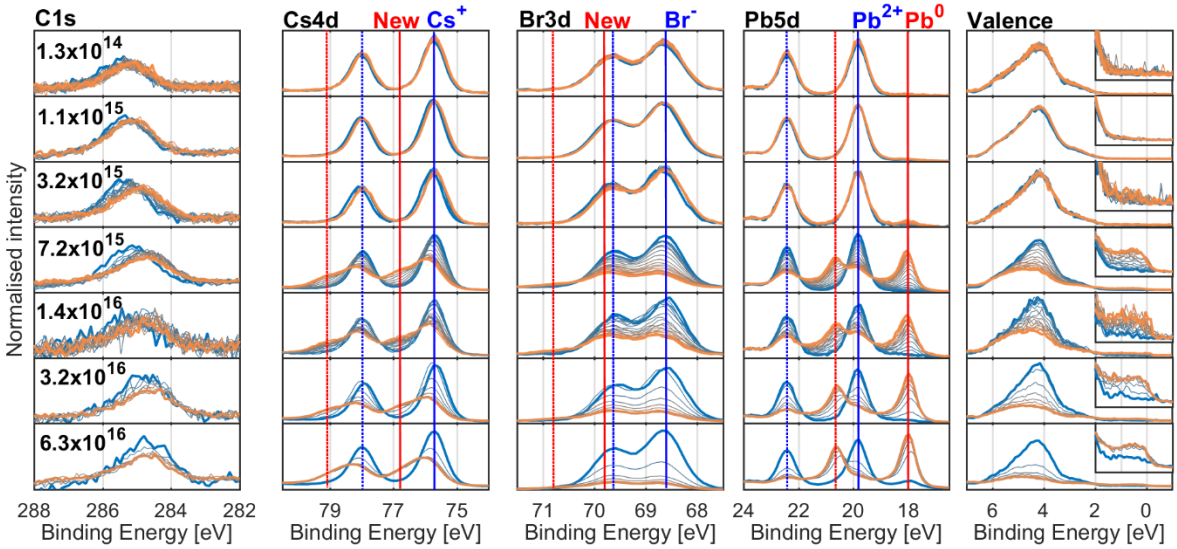

Figure S10: The C1s, Cs4d, Br3d, Pb5d and valence band spectra recorded for a $CsPbBr_3$ as a function of time (blue: start, orange: end) for the C1s, Cs4d, Br3d, Pb5d core level and valence band, normalised and calibrated to total Pb5d at 19.8 eV. Measured at SOLEIL (450 mA) using a photon energy 3000 eV.

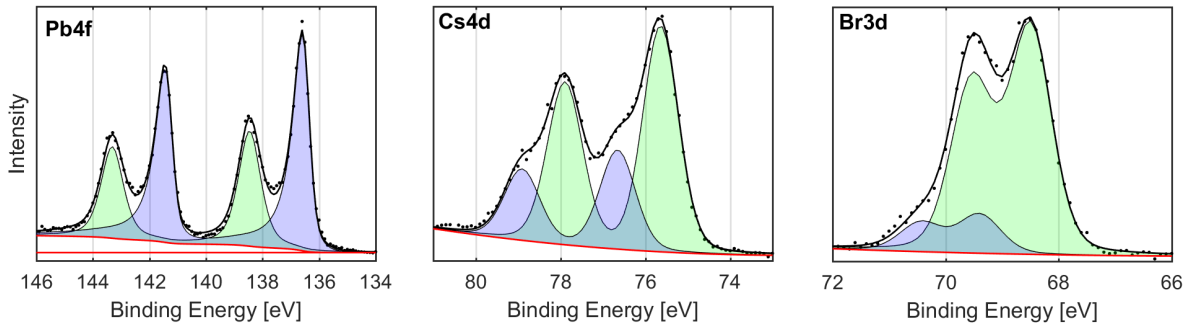

Figure S11: The Pb4f, Cs4d and Br3d fits of the $CsPbBr_3$ sample after 95 minutes irradiation at a X-ray flux density of $1.42x10^{16}$ photons/s/cm².

Chemical ratios

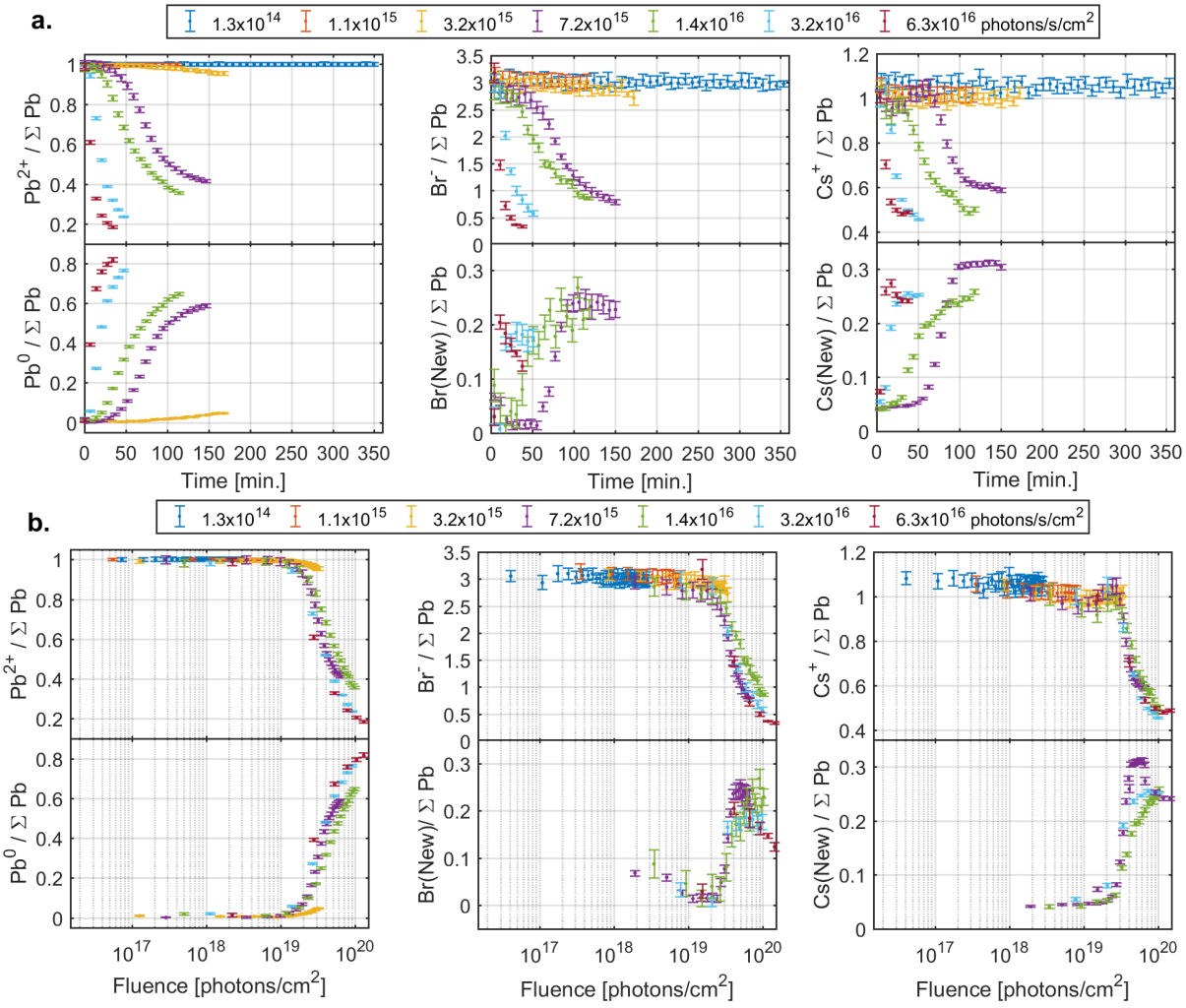

*Figure S12: The ratio of the initial signals (top row) and new signals (bottom row) of the Pb4f (left column), Br3d (middle column) and Cs4d (right column) core levels intensity normalised to total Pb4f intensity. Plotted against time (**a**) and fluence (logarithmic scale) (**b**). The Br3d and Cs4d signals were calibrated by setting the initial Br/Pb and Cs/Pb ratio to 3 and 1, respectively.*

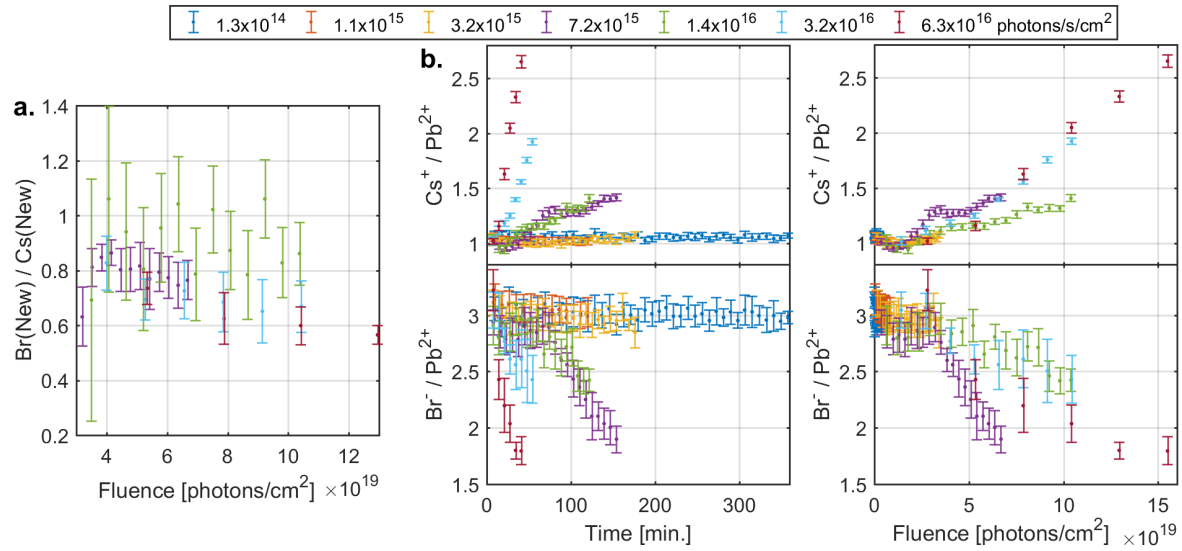

*Figure S13: **a**) The ratio of the new signals of the Br3d and Cs4d core level after degradation has begun. **b**) The Cs^+ component of Cs4d core level (top row) and the Br^- component of Br3d core level (bottom row) normalised to Pb^{2+} component of Pb4f against time (left column) and fluence (right column). The Br3d and Cs4d signals were calibrated by setting the initial Br/Pb and Cs/Pb ratio to 3 and 1, respectively.*

CsBr reference

Table S6: The binding energies and core to core binding energy differences of CsBr given in eV.

$Cs3d_{5/2}$	$Cs4d_{5/2}$	$Br3d_{5/2}$	$Cs3d_{5/2}$ - $Br3d_{5/2}$	$Cs4d_{5/2}$ - $Br3d_{5/2}$
725.32	76.39	69.20	656.13	7.19

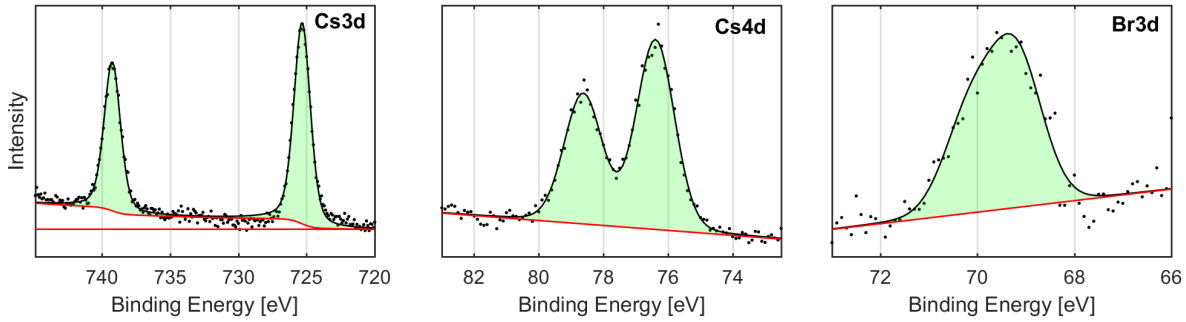

Figure S14: The fits of the Cs3d, Cs4d and Br3d core levels of a CsBr sample. Measured using AlKα on a Physical Electronics Quantera II with a pass energy of 55 eV and step size of 0.1 eV.

References

1 J. H. VanSant, *Conduction Heat Transfer Solutions*, Lawrence Livermore National Lab, CA (USA), 1983.